Calcif Tissue Int (1996) 58:9–16

Calcified
Tissue
International

Laboratory Investigations

Fourier Transform Infrared Spectroscopy of the Solution-Mediated Conversion of Amorphous Calcium Phosphate to Hydroxyapatite: New Correlations Between X-Ray Diffraction and Infrared Data

S. J. Gadaleta,[1] E. P. Paschalis,[2] F. Betts,[2] R. Mendelsohn,[1] A. L. Boskey[2]

[1]Department of Chemistry, Rutgers University, Newark, New Jersey 07102
[2]Department of Ultrastructural Biochemistry, The Hospital for Special Surgery, 535 East 70th Street, New York, New York 10021

Received: 17 January 1995 / Accepted: 26 May 1995

Abstract. Fourier Transform infrared spectroscopic analysis of maturing, poorly crystalline hydroxyapatite (HA) formed from the conversion of amorphous calcium phosphate (ACP) at constant pH or variable pH show only subtle changes in the ν_1, ν_3 phosphate absorption region (900 cm^{-1}–1200 cm^{-1}). This region is of interest because it can be detected by analysis of mineralized tissue sections using FT-IR microscopy. To evaluate the subtle spectral changes occurring during the maturation, second derivatives of the spectra were calculated. HA formed at constant pH showed little or no variation in the second derivative peak positions with bands occurring at 960 cm^{-1}, 985 cm^{-1}, 1030 cm^{-1}, 1055 cm^{-1}, 1075 cm^{-1}, 1096 cm^{-1}, 1116 cm^{-1}, and 1145 cm^{-1}. These bands can be assigned to molecular vibrations of the phosphate (PO_4^{3-}) moiety in an apatitic/stoichiometric environment of HA. In contrast, during the early stages of maturation of the HA formed at variable pH, second derivative peak positions occurring at 958 cm^{-1}, 985 cm^{-1}, 1020 cm^{-1}, 1038 cm^{-1}, 1112 cm^{-1}, and 1127 cm^{-1} shifted in position with maturation, indicating that the environment of the phosphate species is changing as the crystals mature. Peaks at 1020 cm^{-1}, 1038 cm^{-1}, 1112 cm^{-1}, and 1127 cm^{-1} were attributable to nonstoichiometry and/or the presence of acid phosphate-containing species. This concept was supported by the lower Ca:P molar ratios measured by chemical analysis of the synthetic material made at variable pH. Using the second derivative peak positions as initial input parameters, the ν_1, ν_3 phosphate region of the synthetic HAs prepared at constant pH were curve fit. X-ray diffraction patterns of these same materials were also curve fit to calculate the changes in crystallinty (size/perfection) in the c-axis 002 reflection as well as the 102, 210, 211, 112, 300, 202, and 301 planes. Linear regression analysis showed that the changes in the percent area of the underlying bands at 982 cm^{-1}, 999 cm^{-1}, 1030 cm^{-1}, 1075 cm^{-1}, 1096 cm^{-1}, 1116 cm^{-1}, and 1145 cm^{-1} were correlated with changes in crystallinity in one or more of the reflection planes. It is suggested that a combination of second-derivative and curve-fitting analysis of the ν_1, ν_3 phosphate contour allows the most reproducible evaluation of these spectra.

Key words: FT-IR spectroscopy — Hydroxyapatite — Second-derivative spectroscopy — X-ray diffraction — Phosphate species.

The mineral phase in calcified tissues has been extensively studied by infrared (IR) spectroscopy [1–5]. These and other ultrastructural studies [6–8] show this mineral to be a poorly crystalline, carbonate-containing analog of the naturally occurring mineral, hydroxyapatite (HA). Group theoretical analyses of the phosphate modes, coupled with experimental data from isotopically substituted phosphate derivatives, provide a sound basis for spectral assignments of the underlying bands in highly crystalline HA [3, 9–11]. However, assignments for the poorly crystalline biologic apatites and their synthetic analogs which have broad, relatively featureless contours [1, 7, 12, 13] have been more difficult to make. Recently, Fourier transform infrared spectroscopy (FT-IR) has been used to examine HA in both model systems and in calcified tissues [14]. The dramatic increase in the signal-to-noise (S/N) ratio and speed in data acquisition realized with current technology enable the use of data reduction techniques such as Fourier self-deconvolution, curve fitting, and second derivative spectroscopy. The use of these methods allows the determination of underlying bands in the spectra of biologic apatites and their synthetic analogs. In the current work, attention is focused on the ν_1, ν_3 phosphate contour (900–1200 cm^{-1}) as it is readily accessible in studies of mineralized tissues using an FT-IR microscope.

The broad nature of this contour in biologic HA results from factors such as vacancies in the HA lattice [1, 15] and symmetry lowering (the removal of degeneracies) due to the substitution of ions such as CO_3^{2-}, HPO_4^{2-}, Na^+, and Mg^{+2} either in the HA lattice or on the surface of the particle [13, 16, 17]. To characterize spectral changes of the phosphate contour in poorly crystalline biologic apatites, it is necessary to first examine and describe changes in the structure and composition of appropriate model HA compounds. To

Correspondence to: A. L. Boskey

accomplish qualitative and quantitative determination of the variations in the broad FT-IR contours of poorly crystalline HA, three data reduction techniques have been used, namely, Fourier self-deconvolution (FSD) [1], curve fitting [2], and derivative spectroscopy [5, 9]. Fourier self-deconvolution requires the subjective choice of line-narrowing parameters such as the full width at half-height (FWHH) of the underlying bands being deconvolved, and the ratio of the band widths before and after deconvolution. When properly employed, FSD has the potential to preserve band intensities and provides useful information about the positions and relative amplitudes of the underlying peaks. Curve fitting also requires the input of several subjective parameters such as the position, number, and shape (gaussian, lorentzian, or a mixture thereof) of the underlying bands as well as the criteria for convergence in fitting the calculated to the observed spectrum. This method provides the most information about the underlying peaks by calculating the height, width, amplitude, area, and position of each component. Second-derivative spectroscopy has the advantage of being a mathematically objective process. However, it has been empirically found that with each order of derivation, the S/N level drops by a factor of 3–5 [18–20]. Nevertheless, peak positions provide information about the existing molecular species and are sensitive to environmental changes with respect to the species being analyzed.

Pleshko et al. [2] correlated the percent area of one of the subcomponents in the ν_1, ν_3 phosphate (900–1200 cm^{-1}) region with changes in the particle size in the c-axis dimension of synthetic HA as measured by X-ray diffraction (XRD) line broadening analysis. The goal of the current investigation was to establish additional correlations between infrared and X-ray parameters and to provide further insight into the origins of the spectral features in the ν_1, ν_3 phosphate contour of maturing poorly crystalline HA.

Materials and Methods

Synthetic Apatites

Two methods were used to synthesize poorly crystalline HA *in vitro*. In method one, three volumes of 0.04 M $CaCl_2$ in 0.15 M Tris-(hydroxymethyl)-aminomethane (Tris) buffer and three volumes of 0.036 M Na_2HPO_4 in Tris buffer were diluted with four volumes of Tris buffer and mixed with constant stirring at room temperature [21]. The pH was monitored and maintained at 7.4 throughout the reaction by the dropwise addition of dilute NH_4OH. In method two, 1400 ml of 0.022 M $CaCl_2$ and 600 ml of 0.036 M Na_2HPO_4, both prepared in 0.15 M Tris buffer at pH 7.4, were mixed with constant stirring at room temperature. Upon mixing, the pH of the solution immediately dropped to 6.90 and was monitored but not adjusted during the reaction. Though no carbonate salts were used in the syntheses, no precautions were taken to exclude atmospheric CO_2 from either preparation. Both reactions were carried out for a maximum time of 3 weeks. Aliquots were withdrawn at T = O, then every 30 minutes for the first 4 hours. Subsequent aliquots were taken at T = 24 hours and T = 3 weeks. Precipitates were filtered within 2 minutes through a medium porosity fritted glass filter, washed with ammoniated (pH 10) water to remove unreacted salts while preventing dissolution and reprecipitation, dried with spectroscopic grade acetone, and lyophilized for 24 hours. Although washing at pH 10 probably removed some of the surface acid phosphate, it was an essential protocol as the presence of NaCl would have interfered with the XRD analysis.

Spectroscopic and X-Ray Analyses

Crystals were analyzed by FT-IR as KBr pellets (400:1 (KBr:HA), w:w) using a BioRad FTS-40 Infrared Spectrometer (Cambridge, MA). Routinely, 256 interferograms collected at 4 cm^{-1} resolution were co-added and the resultant interferogram Fourier transformed.

XRD patterns were recorded on Siemens D500 Powder Diffractometer (Iselin, NJ). The samples were ground to obtain a relatively uniform particle size, placed into an aluminum sample holder, and scanned in 0.05° intervals between 20° and 37° (2Θ) using Ni-filtered Cu-Kα radiation with a minimum of 8,000 counts per interval.

Calcium-to-Phosphate (Ca:P) Ratios

Precipitates from each time point were dissolved in 2 N HCl (1 mg/10 ml) and analyzed for Ca [22] and PO_4 [23] contents.

Carbonate-to-Phosphate (CO_3^{2-}:P) Ratio

Relative carbonate content was calculated from FT-IR spectra by dividing the integrated area of the ν_2, region (830–1200 cm^{-1}) of the CO_3^{2-} ion by the integrated area of the ν_1, ν_3 phosphate region (900–1200 cm^{-1}).

Aggregate Size Separation

HA aggregates from a typical experiment (T = 24 hours) were used to examine the effect of size on the FT-IR absorbance spectra. HA powders were successively sieved through a series of mesh sizes (300–45 μm). The samples were then mixed with preground KBr to avoid further changes in aggregate size from grinding. The samples were then analyzed by FT-IR using the protocol previously mentioned.

Data Analysis

The derivative and curve fitting algorithms were performed with software developed at the National Research Council of Canada, Ottawa. Raw FT-IR absorbance spectra of the HA samples were baseline corrected between 800 and 1300 cm^{-1}. Second-derivative spectra were calculated with a break point of 0.6. The number and position of the obtained peaks were used as initial input parameters in the curve-fitting algorithm. A mixed gaussian-lorentzian bandshape was used to fit the contours. The percent areas of the underlying bands calculated by the curve-fitting algorithm were reproducible to better than 2%, provided that the input parameters had the same initial values and were input in the same sequence. XRD patterns were smoothed prior to curve fitting with a gaussian function. The smoothing algorithm did not alter the characteristics of the pattern but did eliminate noise distortions. To obtain information about the crystallite thickness along the various axes and planes of HA, the FWHH of the 002, 211, 112, 300, 202, 102, 210, and 301 reflection planes for each timepoint was calculated using the curve-fit XRD patterns. The initial peak positions in the region between 2θ = 24° and 37° were obtained from the Joint Committee on Powder Diffraction Standards [24] listed values for HA. Correlations between FT-IR and X-ray data were calculated by linear regression.

Results

Figure 1 illustrates the subtle time-dependent changes in the absorbance spectra of the ν_1, ν_3 phosphate region (900–1200 cm^{-1}) of the HA synthesized by methods one and two. In both cases the first spectrum (T = 0) exhibits a broad, relatively featureless contour characteristic of amorphous calcium phosphate (ACP), the precursor to HA in these experiments. Upon conversion to poorly crystalline HA (T = 30 minutes), the spectra exhibit a contour with several

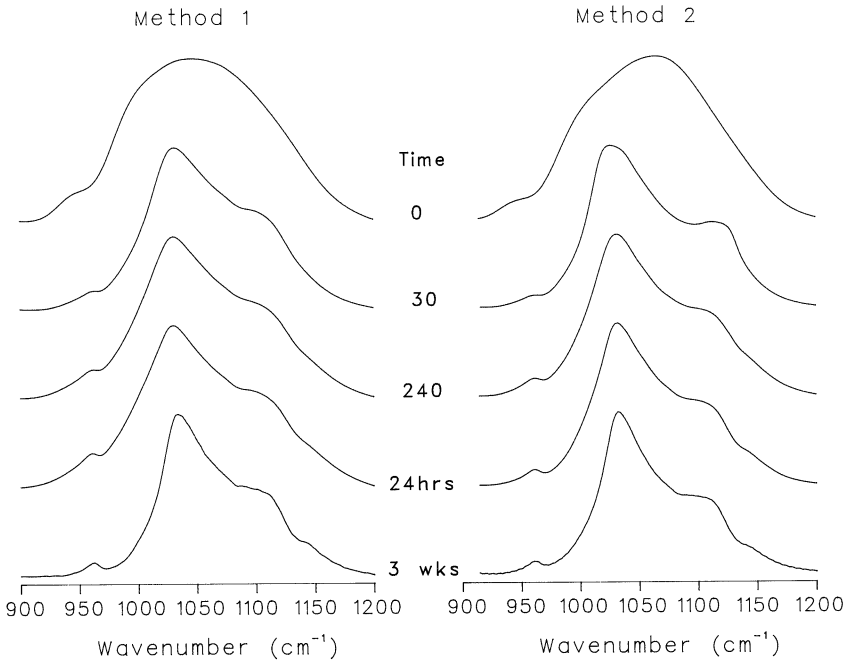

Fig. 1. Typical absorbance spectra of the ν_1, ν_3 phosphate region of the HA synthesized by method one and method two. In method one, the pH was fixed at 7.4. In method two, the pH was allowed to vary throughout the reaction. Times (minutes) shown are the times when the aliquots were withdrawn.

visible peaks and shoulders. As the time in solution increases, the spectra undergo a general sharpening.

To enhance the visibility of the changes in the FT-IR absorbance spectra accompanying maturation of the crystals, second-derivative spectroscopy was used to better define the underlying bands. Figure 2 illustrates the second-derivative spectra of the HA synthesized by each method from T = 30 minutes to T = 24 hours. The spectra of all time points from method one exhibit peaks at 960 cm^{-1}, 985 cm^{-1}, 1030 cm^{-1}, 1055 cm^{-1}, 1075 cm^{-1}, 1096 cm^{-1}, 1116 cm^{-1}, and 1145 cm^{-1} which remain at approximately the same position throughout the reaction. However, the broad single peak at 985 cm^{-1} develops into two distinct peaks centered at 982 cm^{-1} and 999 cm^{-1} as the time in solution increases. For the HAs synthesized by method two, the spectra of early time points (T < 210 minutes) exhibit peaks distinct from those in method one, indicating that the molecular species giving rise to these peaks are also different. At T = 30 minutes, peaks are seen at 959 cm^{-1}, 985 cm^{-1}, 1020 cm^{-1}, 1038 cm^{-1}, 1055 cm^{-1}, 1075 cm^{-1}, 1112 cm^{-1}, and 1127 cm^{-1}. During the first 4 hours of the reaction, the bands shift to positions within ±2 cm^{-1} of the HAs prepared by method one. The peak positions seen in these spectra are summarized in Table 1 along with assignments based on literature values for PO_4^{3-} and HPO_4^{2-}.

The characteristics of the mineral as determined by XRD line broadening analysis were used to obtain information about the size/perfection of the crystals. Figure 3 illustrates the diffraction patterns of ACP (T = 0) and poorly crystalline HA crystals from both methods. The features of interest in the XRD patterns consist of a broad contour between 2Θ = 27–37°, and an isolated peak centered at 25.89° resulting from the 002 reflection of HA. The HA patterns exhibit a general sharpening with time.

To correlate the subtle changes in the FT-IR absorbance spectra with those of the XRD patterns, a curve-fitting algorithm was used to calculate the underlying components of both the FT-IR and X-ray data for HA prepared by method one. Figure 4a and b illustrate typical curve fit data of the FT-IR spectra and XRD patterns of the poorly crystalline HA at T = 24 hours. Tables 2a and b illustrate, respectively, the FWHH of the XRD peaks and the percent areas

Fig. 2. Second-derivative spectra of the ν_1, ν_3 phosphate region of the HA synthesized by method one and method two as shown in Figure 1. In method one, the pH was fixed at 7.4. In method two, the pH was allowed to vary throughout the reaction. Times (minutes) shown are the times when the aliquots were withdrawn.

of the FT-IR subbands which were observed in a typical experiment. The percent area of the FT-IR subbands from both method one experiments were plotted against the FWHH of the corresponding X-ray diffraction peaks to ob-

Table 1. Second-derivative peak positions (cm^{-1}) in the ν_1, ν_3 phosphate region and their assignments from literature values

Method one $T \geqslant 30$[a]	Assignments	Method two 30[a] $\leqslant T \leqslant 210$[a]	Assignments
960	ν_1 PO_4^{3-} [4, 14]	959	ν_1 PO_4^{3-} [4, 14]
982, 985	PO_4^{3-} in HA (980 cm^{-1}) [3] or PO_3 symmetric stretch in Brushite (984 cm^{-1}) [27]	982, 985	PO_4^{3-} in HA (980 cm^{-1}) [3] or PO_3 symmetric stretch in Brushite (984 cm^{-1}) [27]
999	ν_3 Asymmetric stretch ~1004 cm^{-1} [14]	999	ν_3 Assymetric stretch ~1004 cm^{-1} [14]
		1020	ν_3 PO_4 from nonstoichiometric apatite [1]
1030	ν_3 PO_4^{3-}, occurring in stoichiometric apatites [1, 3]		
		1038	ν_3 PO_4^{3-} not part of apatitic structure in OCP [26]
1055	ν_3 PO_4^{3-} [14]	1055	ν_3 PO_4^{3-} [14]
1075	ν_3 PO_4^{3-} [3, 14]	1075	ν_3 PO_4^{3-} [3, 14]
		1112	Found in freshly precipitated poorly crystalline HA [1]
1096	ν_3 PO_4^{3-} [3, 14]		
1116	Found in mature poorly crystalline HA [1]		
		1127	ν_6' and ν_6'' PO_3^- degenerate stretch of HPO_4^{2-} ions in brushite [27]
1145	Found in HPO_4^{2-} containing apatite [1], possibly due to surface acid phosphate that was not entirely removed		

[a] Minutes

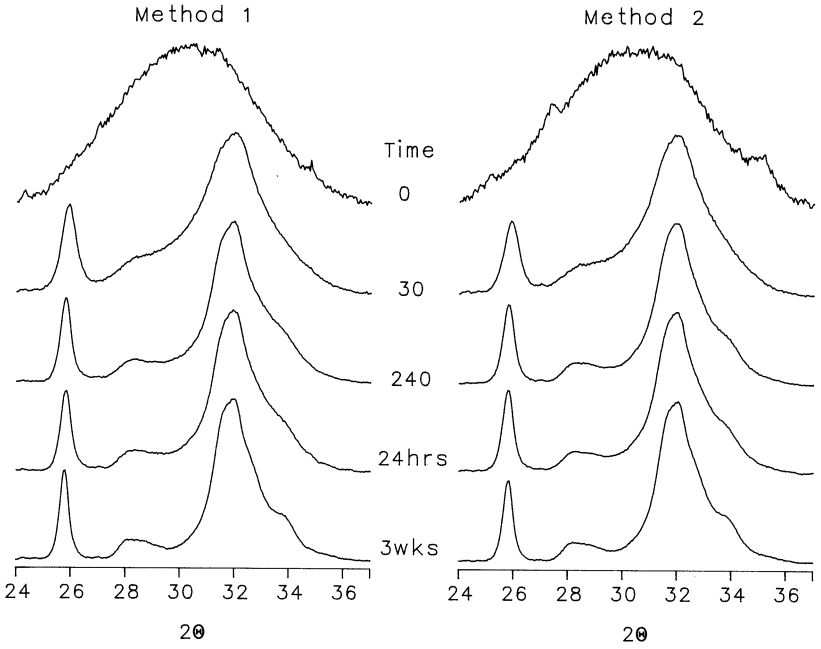

Fig. 3. X-ray diffraction patterns of the HA synthesized by method one and method two. In method one, the pH was fixed at 7.4. In method two, the pH was allowed to vary throughout the reaction. Times (minutes) shown are the times when the aliquots were withdrawn.

tain spectra-structure correlations. Several strong ($r \geqslant 0.6$) linear correlations of subband area with crystallinity were noted and are listed in Table 3. Specifically, the percent areas of the 1030 cm^{-1}, 1096 cm^{-1}, and 1116 cm^{-1} subbands, all associated with PO_4^{3-} in stoichiometric HA, decreased with decreasing FWHH of specific X-ray reflections. The percent areas of the 982 cm^{-1}, 999 cm^{-1}, 1075 cm^{-1}, and 1145 cm^{-1} subbands all increased with decreasing FWHH of certain X-ray reflections. It is important to note that the percent area of the 1055 cm^{-1} band remained relatively constant. No correlations ($R > 0.6$) were observed for the 210, 301, and 112 reflections.

The Ca:P and CO_3^{2-}:P molar ratios of the HA synthesized in methods one and two are presented in Table 4. The Ca:P molar ratios of the samples prepared by method two have a lower value, and exhibit a greater change than the samples prepared by method one. The pH values of selected aliquots from methods one and two are shown in Table 4. HA prepared by both methods exhibits a progressive increase in the CO_3^{2-}:P with time.

To verify that the spectral changes were not simply due to changes in aggregate size of the HA crystals, the absorbance spectra of a HA sieved to different sizes were analyzed (Fig. 5). No appreciable changes in the absorbance spectra can be detected by visual inspection of the contour. Second-derivative spectra of the samples (Fig. 5), while varying in S/N ratios, show no changes in the position of the peaks with increasing aggregate size. Similarly, there were no significant changes in the percent areas of the underlying bands (not shown).

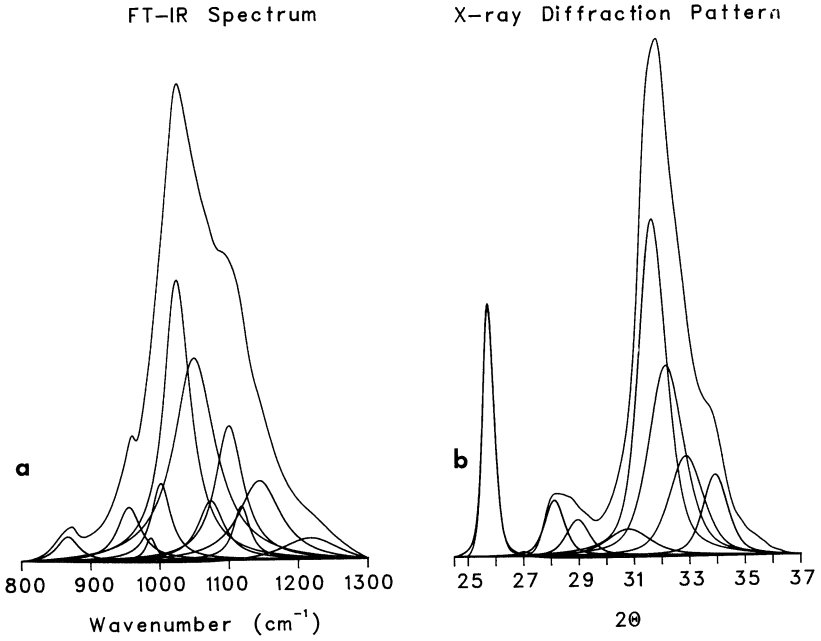

Fig. 4. Curve fit of the FT-IR spectra and X-ray diffraction patterns of the HA (24-hour) synthesized by method one. Input parameters for the FT-IR spectra were obtained from the second derivatives. Parameters for the XRD patterns were obtained from the JCPDM [24] values for HA.

Table 2a. Typical line broadening analysis of poorly crystalline HA prepared by method one. FWHH were calculated from the curve fits of the hkl[a] reflections of the X-ray diffraction patterns

Time[b]	FWHH	FWHH	FWHH	FWHH	FWHH	FWHH	FWHH	FWHH
	211	112	300	202	002	102	210	301
30	1.66	0.968	2.35	1.69	0.665	0.838	1.11	4.83
60	1.50	1.07	2.28	1.80	0.589	0.952	1.65	2.23
90	1.44	0.821	1.91	1.74	0.559	1.02	1.46	2.36
120	1.36	0.841	2.01	1.42	0.514	0.789	1.82	1.06
150	1.35	0.734	1.80	1.43	0.487	0.724	2.01	0.682
180	1.28	0.732	1.90	1.18	0.482	0.868	1.37	2.01
210	1.29	0.827	1.84	1.28	0.479	0.776	1.61	1.15
240	1.27	0.804	1.82	1.32	0.473	0.752	1.54	1.39
24 hours	1.19	0.795	1.72	1.16	0.432	0.695	1.42	1.29
3 weeks	0.984	0.655	1.52	1.02	0.312	0.602	1.32	1.01

[a] Miller indices refer to crystal planes in the reciprocal lattice
[b] Minutes or as otherwise indicated

Table 2b. Typical percent areas of the underlying FT-IR bands calculated from the curve fit spectra of poorly crystalline HA prepared by method one

Time[a]	% Area	% Area	% Area	% Area	% Area	% Area	% Area	% Area	% Area	% Area
	960cm^{-1}	982cm^{-1}	999cm^{-1}	1030cm^{-1}	1055cm^{-1}	1075cm^{-1}	1096cm^{-1}	1116cm^{-1}	1145cm^{-1}	1200cm^{-1}
30	2.307	0.5543	2.927	28.66	28.17	4.681	15.95	5.690	5.003	5.030
60	2.516	0.3489	1.280	30.15	29.73	3.887	14.84	7.388	3.339	5.642
90	2.606	0.4116	1.734	30.09	28.04	4.332	14.63	6.728	4.361	5.987
120	2.460	0.6771	3.625	28.70	26.24	4.009	14.25	5.589	4.508	8.787
150	1.509	0.4870	2.535	30.84	28.97	4.762	14.95	5.909	3.748	5.309
180	1.932	0.5928	3.456	29.09	30.25	4.643	14.72	4.415	5.352	4.433
210	2.358	0.6567	4.018	27.53	30.01	5.607	13.71	4.144	5.525	5.139
240	2.880	0.7243	4.445	25.27	29.12	5.638	12.57	3.296	9.281	5.079
24 hours	4.103	0.7592	4.794	23.95	27.23	5.022	12.01	2.836	11.18	6.118
3 weeks	8.521	0.80	5.623	23.01	26.25	6.123	11.26	2.325	10.61	6.750

[a] Minutes

Discussion

The results of this study demonstrate the capabilities of combining second-derivative spectroscopy and curve-fitting in the analysis of poorly crystalline apatites. They also demonstrate that the variations in FT-IR spectra of synthetic apatites are due to both compositional changes and changes in crystallite thickness along several planes, but are not attributable to the aggregate size of the materials being analyzed. Further, they suggest that because of the large number of dependent correlations, it is better to present data as percent subband areas rather than calculating particle sizes.

The inherent objectivity of second-derivative spectroscopy provides a method of analysis relatively free of arti-

Table 3. Linear correlations[a] between X-ray diffraction full width at half-height and the % area of FT-IR subbands from HA prepared by method one

	FT-IR subbands						
hkl[a]	982 cm^{-1}	999 cm^{-1}	1030 cm^{-1}	1075 cm^{-1}	1096 cm^{-1}	1116 cm^{-1}	1145 cm^{-1}
002	(+) 0.613	(+) 0.792	(−) 0.606	(+) 0.625	(−) 0.763	(−) 0.792	(+) 0.663
102	(+) 0.688	(+) 0.717	(−) 0.704		(−) 0.652	(−) 0.791	(+) 0.658
211				(+) 0.695	(−) 0.746	(−) 0.775	(+) 0.649
300				(+) 0.664		(−) 0.660	
202				(+) 0.606		(−) 0.702	

[a] Only linear correlations with r ⩾ 0.6 are shown. (+) Refers to increasing % area of FT-IR subband with decreasing FWHH of XRD peaks; (−) refers to decreasing % area of FT-IR subband with decreasing FWHH of XRD peaks
[b] Miller indices referring to the crystal planes in the reciprocal lattice

Table 4. Ca:P (measured analytically) and CO_3^{2}:P (measured spectroscopically) ratios for synthetic HA prepared by methods one and two

	Method one			Method two		
Time[a]	Ca:P ratio (molar ratio)	CO_3:P ratio (ratio of IR absorbances) × 10^{-3}	pH	CA:P ratio (molar ratio)	CO_3:P ratio (ratio of IR absorbances) × 10^{-3}	pH
0	1.53 ± 0.02	NA	7.4	1.38 ± 0.06	NA	6.90
30	1.61 ± 0.04	3.92	7.4	1.49 ± 0.07	5.19	
60	1.64 ± 0.01	3.70	7.4	1.57 ± 0.21	6.37	6.95
90	1.65 ± 0.04	4.54	7.4	1.47 ± 0.07	4.72	
120	1.59 ± 0.01	5.16	7.4	1.53 ± 0.12	7.10	6.94
150	1.58 ± 0.03	5.25	7.4	1.51 ± 0.11	7.15	
180	1.61 ± 0.09	5.68	7.4	1.48 ± 0.10	7.58	6.94
210	1.58 ± 0.02	5.84	7.4	1.57 ± 0.14	7.45	
240	1.59 ± 0.01	6.26	7.4	1.54 ± 0.09	8.21	6.95
24 hour	1.58 ± 0.02	6.93	7.4	1.56 ± 0.22	7.64	
3 week	1.65 ± 0.01	7.00	7.4	1.60 ± 0.09	8.32	

facts. To eliminate distortion derived from high-frequency noise, second-derivative spectra were calculated from interferograms in which only the first 60% (break point 0.6) of the data points were used. This cutoff value was obtained by estimating the point at which the amplitude of the interferogram began to increase (detection of a real signal) from the relatively constant amplitude (random noise) seen at both ends of the interferogram [18–20]. Elimination of the remaining 40% resulted in the reduction of high-frequency noise and did not effect the general features of the resulting second-derivative spectrum. Coupling second-derivative spectroscopy with a curve-fitting algorithm provided a more reliable starting point in the analysis of the broad contours. As mentioned earlier in this manuscript, curve fitting requires the input of several subjective parameters, including the number and position of underlying peaks in a contour. Using the position and number of peaks in a second-derivative spectrum makes the choice of input parameters less arbitrary.

Second-derivative spectroscopy has recently been utilized by Leung et al. [5, 9] in the assignment of factor group elements to peak positions in the ν_1, ν_3, and ν_4 regions of HA. Although Leung et al.'s study provides useful information concerning well crystalline HA, the apatites were synthesized at high temperature, resulting in very large/perfect crystals; consequently, this study cannot be directly used to characterize the poorly crystalline HA commonly found in biologic tissue [25]. It is important to note that the relatively constant peak positions at 960 cm^{-1}, 1030 cm^{-1}, 1055 cm^{-1}, 1075 cm^{-1}, 1096 cm^{-1}, and 1116 cm^{-1} in the second-derivative spectra of the poorly crystalline HA synthesized in method one have all been assigned to phosphate vibrations in the apatitic environment of crystalline HAs [1, 3, 4, 9, 10]. The minor bands at 982 cm^{-1}, 985 cm^{-1}, and 1200 cm^{-1} have not conclusively been assigned. The constant position of the bands in the second-derivative spectra during maturation of the HA indicates that the environment of the phosphate species is not changing as the crystals develop. In contrast, the second-derivative peaks of the early HA samples (T < 210 minutes) synthesized by method two, in which pH varied with time, do change during maturation. The peaks found at 1020 cm^{-1}, 1038 cm^{-1}, 1112 cm^{-1}, 1127 cm^{-1} seen in the T < 210 minute samples from the HA prepared by method two have been assigned to phosphate vibrations (see Table 1) in nonstoichiometric environments of freshly precipitated apatites [1] and/or other acid phosphate containing calcium phosphate phases such as octacalcium phosphate (OCP), monetite, and brushite [1, 3, 4, 26, 27]. Thus, the detection of these bands in the second-derivative spectra, coupled with the drop in pH, indicates the presence of a phosphate moiety in a nonapatitic/acid phosphate environment at early stages of maturation in the apatites synthesized by method two.

The low Ca:P ratios seen in the materials synthesized by method two might be due to the presence of brushite, monetite, and OCP, or to the presence of nonstoichiometric and/or calcium-deficient apatites. The absence of additional spectral and XRD characteristics, which would confirm the presence of specific nonapatitic calcium phosphate phases, suggests the latter is more likely. The ability to distinguish different phosphate environments accompanying the maturation of synthetic HAs provides a method of analysis that

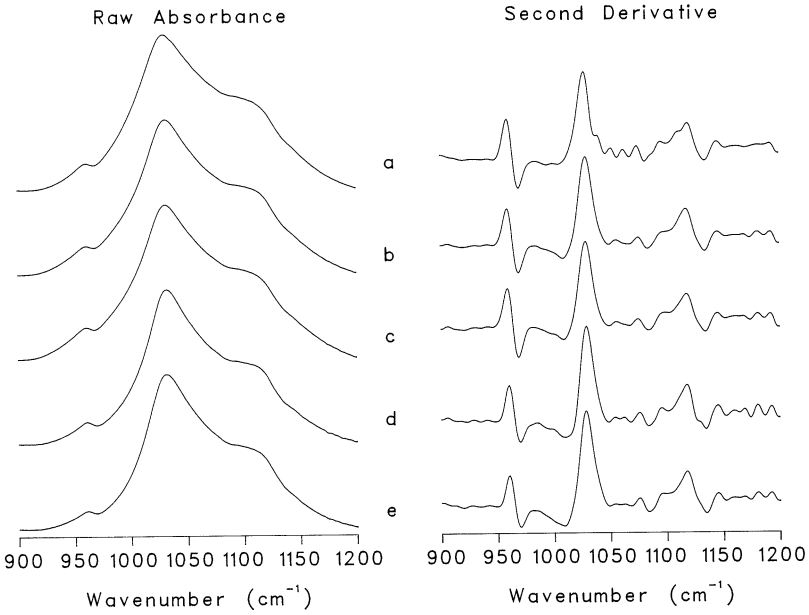

Fig. 5. FT-IR absorbance and second-derivative spectra are not affected by aggregate size of HA. **(a)** aggregate > 300 μm; **(b)** 300 μm < aggregate < 150 μm; **(c)** 150 μm < aggregate < 75 μm; **(d)** 75 μm < aggregate < 45 μm; **(e)** 45 μm > aggregate < 26 μm.

can be extended to the analysis of the mineral phase in calcified tissue.

The increase of the CO_3^{2-}:P ratio in the materials synthesized by method two is probably due to the incorporation of atmospheric carbonate into the apatite lattice. It should be noted that the carbonate band in the 830 cm^{-1}–900 cm^{-1} region is superimposed on a broad, low, absorbing acid phosphate band [17] which may contribute to the overall area of what we define as the carbonate component. The HPO_4^{2-} does not appear to make a significant contribution since the second-derivative spectra of method two show a continuous decrease in acid phosphate content denoted by the disappearance of the bands at 1038 cm^{-1} and 1127 cm^{-1} whereas the carbonate-to-phosphate ratio continuously increases at time points beyond 90 minutes.

The variations in peak positions, Ca:P ratio, and CO_3^{2-}:P ratio may be ascribed to changes in the structural composition of the maturing HA crystals or to the presence of ionic species such as HPO_4^{2-} and CO_3^{2-} on the surface of the crystals. Although washing the precipitates with pH 10 water removed most of the surface active species, the methods used in the current work are not capable of assessing the contributions of such species.

The combination of second-derivative and curve-fit IR spectra and XRD diffraction patterns allowed the identification of both compositional changes and changes in crystallite size. Here, crystallite size indicates the particle thickness that leads to broadening of the XRD patterns rather than the aggregate size of the apatite particles. It has been suggested that variations in aggregate size can cause spectral distortions related to Christiansen scattering [1]. The results from this study indicate that spectral parameters used to characterize the mineral were not affected by the aggregate size of the particles.

Pleshko et al. [2] have previously shown that variations in the percent area of the underlying components in the ν_1, ν_3 phosphate contour were related to increases in crystallite size and perfection in the c-axis direction. In particular, an underlying FT-IR band at 1060 cm^{-1} was shown to be inversely related to the crystal size, as deduced by XRD line broadening analysis of the c-axis 002 peak. The results of the current study, however, do not demonstrate an inverse relation between the percent area of an FT-IR subband at 1060 cm^{-1} with the HA crystal size in the c-axis dimension. This is due primarily to the fact that a different number of bands was used to curve fit the IR contours. Whereas the Pleshko study used a total of six underlying bands to fit the ν_1, ν_3 phosphate region, the present study used nine bands based on the second-derivative spectra of the apatites. With the additional number of bands, the 1060 cm^{-1} component was resolved into a component at 1055 cm^{-1}, which remained constant, one at 1075 cm^{-1} which increased with increased crystal size in the 002, 211, 200, and 202 directions, and one at 1096 cm^{-1} which decreased with increased crystal size in the 002, 102, and 211 directions. Although a minor band centered near 1200 cm^{-1} was needed to properly fit the FT-IR contours, it was not correlated with any X-ray reflections. Our results indicate that the changes in the ν_1, ν_3 region are also related to the variations in the particle size along other crystal planes. Thus, for apatites with a homogeneous phosphate environment, the differences in the particle size can be correlated with corresponding changes in the percent area of the underlying FT-IR bands. Though these relationships complement the findings of Pleshko et al. [2], the results of the present study suggest that consideration of all underlying components offers a more precise description of the maturation of HA crystals.

The observed linear correlations (Table 3) between the FWHH of the XRD reflections and the percent areas of the various IR bands in the ν_1, ν_3 phosphate region are presumably different manifestations (as sensed by the two physical techniques) of the same underlying phenomenon. It is well established that the XRD linewidths, via the Debye Scherrer equation [29], are a direct measure of crystal size/perfection, a narrower line being indicative of a larger and/or a more perfect crystal. The correlation of the IR spectral features with crystal size/perfection is more subtle. The change in the percent areas of the IR subbands reflects altered coupling between the phosphate ν_1, ν_3 bands of the various phosphate ions in a single unit cell as well as in neighboring unit cells. This type of coupling is fairly well understood for simple cases such as interacting methylene

groups in crystalline alkanes and gel state phospholipids [30, 31]. A detailed analysis is precluded in the current case by the relatively low symmetry and disorder of the phosphate groups in the CaP phases. It is to be expected that as the phosphate ions become more uniform (more perfect crystals, larger crystals), the following changes would occur in the spectra: Initially, the bands would be broadened due to inhomogeneous broadening (same vibrational mode, slightly different environments). As the crystal grows and becomes more perfect, the coupling would produce new bands at positions that would become progressively sharper and gain in intensity.

Acknowledgments: This work was supported by NIH Grant AR41325.

References

1. Rey C, Shimizu M, Collins B, Glimcher MJ (1991) Resolution-enhanced Fourier transform infrared spectroscopy study of the environment of phosphate ion in the early deposits of a solid phase calcium phosphate in bone and enamel and their evolution with age: investigations in the ν_3PO_4 domain. Calcif Tissue Int 49:383–388
2. Pleshko NL, Boskey AL, Mendelsohn R (1991) Novel infrared spectroscopic method for the determination of crystallinity of hydroxyapatite minerals. Biophys J 60:786–793
3. Baddiel CB, Berry EE (1966) Spectra-structure correlations in hydroxy and fluorapatite. Spectrochim Acta 22:1407–1416
4. Fowler BO, Moreno EC, Brown WE (1966) Infra-red spectra of hydroxyapatite, octacalcium phosphate and pyrolysed calcium phosphate. Arch Oral Biol 11:477–492
5. Walters MA, Leung YC, Blumenthal NC, LeGeros RZ, Konsker KA (1990) A raman and infrared spectroscopic investigation of biological hydroxyapatite. J Inorg Biochem 39:193–200
6. Posner AS, Betts F (1975) Synthetic amorphous calcium phosphate and its relation to bone mineral structure. Accts Chem Res 8:273–281
7. Termine JD (1972) Mineral chemistry and skeletal biology. Clin Orthop 85:207–212
8. Posner AS, Blumenthal NC, Boskey AL, Betts F (1975) Synthetic analogue of bone mineral formation. J Dent Res 54:B88–B93
9. Leung Y, Walters MA, LeGeros RZ (1990) Second derivative spectra of hydroxyapatite. Spectrochim Acta 46A:1453–1459
10. Fowler BO (1974) Infrared studies of apatites. I. Vibrational assignments for calcium, strontium, and barium hydroxyapatites utilizing isotopic substitution. Inorg Chem 13:194–206
11. Fowler BO (1974) Infrared studies of apatites. II. Preparation of normally and isotopically substituted calcium, strontium, and barium hydroxyapatites and spectra-structure correlations. Inorg Chem 13:207–214
12. Termine JD, Eanes ED (1972) Comparative chemistry of amorphous and apatitic calcium phosphate preparations. Calcif Tissue Res 10:171–197
13. Blumenthal NC, Betts F, Posner AS (1975) Effect of carbonate and biological molecules on formation and properties of hydroxyapatite. Calcif Tissue Res 18:81–90
14. Bailey RT, Holt C (1989) Fourier transform infrared spectroscopy and characterisation of biological calcium phosphates. In: Hukins DW (ed) Calcified Tissue. Macmillan Press, London, pp 93–119
15. Berry EE (1966) The structure and composition of calcium-deficient apatites. J Inorg Nucl Chem 29:317–327
16. Arends J, Davidson CL (1975) HPO_4^{2-} content in enamel and artificial carious lesions. Calcif Tissue Res 18:65–79
17. Rey C, Renugopalakrishnan V, Collins B, Glimcher MJ (1991) Fourier transform infrared spectroscopic study of the carbonate ions in bone mineral during aging. Calcif Tissue Int 49:251–258
18. Maddams WF, Mead WL (1982) The measurement of derivative IR spectra-I. Background studies. Spectrochim Acta 38A: 437–444
19. Hawkes S, Maddams WF, Mead WL, Southon MJ (1982) The measurement of derivative IR spectra-II. Experimental measurements. Spectrochim Acta 38A:445–457
20. Maddams WF, Southon MJ (1982) The effect of band width and band shape on resolution enhancement by derivative spectroscopy. Spectrochim Acta 38A:459–466
21. Boskey AL, Posner AS (1973) Conversion of amorphous calcium phosphate to microcrystalline hydroxyapatite. A pH-dependent, solution mediated, solid-solid conversion. J Phys Chem 77:2313–2317
22. Willis JB (1960) The determination of metal in blood serum by atomic absorption. Spectrochim Acta 16:259–272
23. Heinonen JK, Lahti RJ (1981) A new and convenient colorimetric determination of inorganic orthophosphate and its application to the assay of inorganic pyrophosphates. Anal Biochem 113:313–317
24. Powder Diffraction File (1960) Joint Committee on Powder Diffraction Standards, Philadelphia, PA
25. Betts F, Blumenthal NC, Posner AS (1981) Bone mineralization. J Crys Growth 53:63–73
26. Berry EE, Baddiel CB (1967) Some assignments in the infrared spectrum of octacalcium phosphate. Spectrochim Acta 23A:1781–1792
27. Berry EE, Baddiel CB (1967) The infra-red spectrum of dicalcium phosphate dihydrate (Brushite). Spectrochim Acta 23A:2089–2097
28. van Wazer JR (1958) Phosphorus and its compounds. Interscience, New York
29. Cullity BD (1956) Elements of x-ray diffraction. Addison-Wesley Publishing Company Inc., Reading, Ma. pp 97–99
30. Senak L, Moore D, Mendelsohn R (1992) CH_2 wagging progressions as IR probes of slightly disordered phospholipid acyl chain states. J Phys Chem 96:2749–2754
31. Snyder RG (1960) Vibrational spectra of crystalline n-paraffins part 1. Methylene rocking and wagging modes. J Mol Spectros 4:411–419